Annular Typhoons in the Western North Pacific

KEKUAN CHU AND ZHE-MIN TAN

Key Laboratory of Mesoscale Severe Weather/Ministry of Education, and School of Atmospheric Sciences, Nanjing University, Nanjing, China

(Manuscript received 23 May 2013, in final form 20 November 2013)

ABSTRACT

Annular hurricanes, characterized by annular structure, are a subset of mature-stage intense tropical cyclones, and they tend to be stronger and persist longer than average tropical cyclones. The characteristics of annular hurricanes in the North Atlantic and eastern-central North Pacific Oceans are well documented by Knaff et al. However, little is known about the annular typhoons in the western North Pacific (WNP). This study investigates the general features of annular typhoons in the WNP based on a 20-yr analysis (1990–2009) of global storm-centered infrared brightness temperature and passive microwave satellite datasets. Similar to annular hurricanes, annular typhoons also only form under a specific combination of environmental conditions, resulting in a quite low occurrence rate (~4%), and only 12 annular typhoons occur during this period. The concentric eyewall replacement is one effective pathway to annular typhoon formation. Three annular typhoons experienced the concentric eyewall replacement within 24 h prior to their annular phases during this period. There are two seedbeds, located east of Taiwan and in the central WNP, for annular typhoon formation within a narrow zonal belt (20°–30°N). The former is conducive to the landfall of annular typhoons, in particular six of the nine annular typhoons that formed in this region eventually made landfall. Because the average time interval between landfall of the annular typhoons and the end of their annular phase is relatively short, about 30 h, they can maintain near-peak intensities and hit the landfalling areas with record intensities. They present a unique threat to eastern Asia but have received little attention from the scientific community so far.

1. Introduction

Knaff et al. (2003, hereafter K03) introduced a new type of tropical cyclones (TCs), named the annular hurricanes (AHs), based on infrared satellite images and reconnaissance aircraft data in the Atlantic and eastern North Pacific Oceans. AHs are generally axisymmetric and characterized by a larger than average circular eye surrounded by a nearly uniform ring of deep convection and lack of spiral rainbands outside this convective ring. AHs are often classified as intense hurricanes (with average intensity of approximately 110 kt, where 1 kt = 0.5144 m s^{-1}), and maintain their peak intensities longer and weaken much slower than typical TCs (Knaff et al. 2008). As a result, the forecasting of the weakening of AHs, once formed, remains a challenging issue.

Environmental factors are assumed to be critical for the formation of AHs. DeMaria (2009) showed that AHs form under the environmental conditions of both low convective instability and low vertical wind shear. K03 summarized that annular hurricanes only formed in very specific environmental conditions, characterized by the combination of 1) weak easterly or southeasterly vertical wind shear, 2) easterly flow and relative cold temperatures at 200 hPa, 3) a narrow range (25.4°–28.5°C) of SSTs that are nearly constant, and 4) a lack of 200-hPa relative eddy flux convergence due to environmental interactions. The individual conditions associated with AHs are quite common, but the simultaneous combination of the environmental conditions is quite rare. As a result, the occurrence of an AH is rare (~4% of all hurricanes in the Atlantic and eastern-central North Pacific). Based on the aforementioned environmental conditions that are necessary for AH occurrence and the unique features on IR imagery, Knaff et al. (2008) developed an objective method to identify AHs. This method has been transitioned to operations and is available to forecasters at the National Hurricane Center in Miami, Florida.

Some mechanisms for AH formation have been reported; however, our understanding of AH formation

Corresponding author address: Dr. Zhe-Min Tan, School of Atmospheric Sciences, Nanjing University, Nanjing 210093, China. E-mail: zmtan@nju.edu.cn

DOI: 10.1175/WAF-D-13-00060.1

and maintenance is far less than complete. Observations show that mesovortices can act as ''mixmasters,'' which efficiently mix the surrounding air into the storm center and transform a smaller eye into a larger eye (K03). Recent idealized numerical simulations indicate that the formation of an AH is attributed to the internal dynamics. For instance, Wang (2008) noted that the formation of an AH is closely related to the interaction between the inner spiral rainbands and the eyewall convection, which is similar to the eyewall replacement in the concentric eyewall. After that, Zhou and Wang (2009) further indicated that the concentric eyewall replacement through bottom-up potential vorticity mixing in the concentric is an efficient pathway for AH to form. Based on observations (Kossin and Sitkowski 2009), the formation of a secondary eyewall, which reaches a quasi-steady state at a larger radius, is also hypothesized as the precursor to annular hurricane formation. However, the relation between concentric eyewall formation and annular TCs need further observational investigation.

As mentioned in K03, annular TCs as a subset of TCs also exist in other TC basins. However, our knowledge on the general characteristics of annular TCs in other TC basins is incomplete. The western North Pacific (WNP) is one of the more active TC areas in the world. Whether annular TCs in the WNP have similarities to those in the Atlantic and eastern-central North Pacific still remains an open question. In this study, the general characteristics of the annular typhoons (ATYs) in the WNP will be investigated. Section 2 will describe the datasets, the details for calculating the environmental conditions, and the methodology used to identify an ATY. The features of ATYs, including their axisymmetry, intensity characteristics, and geographical distribution, will be discussed in section 3. And the environmental conditions for ATYs and the other WNP typhoons will be compared in section 4. Section 5 will discuss the relation between concentric eyewall replacement and annular TC formation. Our main conclusions will be given in the final section.

2. Data and methods

In this study, several datasets are used to examine the characteristics of ATYs in the WNP during the period of 1990–2009. Records from the new Hurricane Satellite (HURSAT) data project and the International Satellite Cloud Climatology Project (ISCCP) B1 geostationary satellite observations (HURSAT-B1; Knapp and Kossin 2007) are utilized to reveal the cloud-top structure of TCs. This dataset collects information of more than 2000 tropical storms with the infrared window channel data from multiple geostationary satellites. These satellite observations are on $0.07° \times 0.07°$ (~8 km) Lagrangian grids at 3-h intervals. They are repositioned on the storm center based on the center-position information provided by the best track datasets.

It should be noted that the spiral rainbands under the cirrus canopy might possibly be invisible in IR imagery when using IR brightness temperatures to determine cloud structures of TCs. Passive microwave data can penetrate the cirrus canopy and detect the convection under the cirrus canopy. Therefore, passive microwave data (HURSAT-MW) is also employed to identify an ATY. The HURSAT-MW dataset is constructed in largely the same manner as HURSAT-B1. However, these passive microwave data have limited spatial coverage and time frequency (about 24 microwave observations per storm); thus, they cannot provide consistent images of TCs.

The TC track and intensity information comes from the best track dataset from the Joint Typhoon Warning Center (JTWC), and the TC translation speed is also calculated based on this best track dataset. The sea surface temperature (SST) determines the amount of sensible and latent heat from the ocean, and is critical for TC formation and evolution (Miller 1958; Malkus and Riehl 1960; Merrill 1988). In this study, the SST at the storm center is linearly interpolated in time and is interpolated in space using bicubic spline interpolation from the weekly optimum interpolation (OI) sea surface temperature (SST) analysis with 1° spatial resolution (Reynolds et al. 2002).

Statistics of the important environmental factors associated with ATYs are extracted from the National Centers for Environmental Prediction–National Center for Atmospheric Research (NCEP–NCAR) global reanalysis dataset in 6-h intervals (Kalnay et al. 1996). Environmental factors include the upper-tropospheric (200 hPa) temperature and zonal wind, the 200–850-hPa vertical wind shear, the 500–850-hPa vertical wind shear, and the 200-hPa relative eddy momentum flux convergence (REFC). The upper-tropospheric temperature is an important thermodynamic control of TC evolution. The environmental wind shear has a significant impact on the structure of hurricanes (Jones 1995; Bender 1997; Frank and Ritchie 1999, 2001; Knaff et al. 2004), and the REFC reflects the interaction between the TC and upper-level midlatitude trough (DeMaria et al. 1993). The REFC is calculated using the same method as in K03. An annular average (radius from 200 to 800 km) is used to calculate the statistics of the above environmental conditions.

Knaff et al. (2008) introduced an objective method to identify AHs based on their unique characteristics in the IR imagery and a set of specific environmental conditions.

Since the environmental conditions necessary for ATY formation in the WNP are still unknown, we use a subjective method to identify ATY as the first step. First, we examined the time versus radius plots of azimuthally averaged IR brightness temperatures of each typhoon during 1990–2009, and then we select possible candidate ATYs. After that, a simple automatic approach is applied to each candidate ATY to exclude those times that are unlikely to be annular. The criteria for this selection include the radius of coldest azimuthally averaged IR brightness temperature (greater than 50 km), the maximum difference between R_c and any azimuthally averaged IR brightness temperature at smaller radii (greater than 15°C), and the maximum surface wind (greater than 80 kt). Finally, visual inspection and qualitative evaluation of the prescreened IR imagery and the microwave imagery (if available) is conducted. An ATY is identified if the storm illustrates an annulus structure over at least a 3-h period, and at the same time there is no organized spiral rainband under the cirrus canopy.

3. General features of annular typhoons

Twelve typhoons in the WNP during 1990–2009 are eventually identified as ATYs. Table 1 lists their beginning and ending times, their durations, and the intensity range of each annular phase, the information about landfall (interpolated from JTWC best track dataset), and the formation regions of ATYs (R1 and R2 are marked in Fig. 5). The occurrence rate of ATYs is close to 4% of all typhoons (with maximum surface wind speeds greater than 64 kt), which is similar to the occurrence rate of AHs (Knaff et al. 2008). Due to the limitations in the temporal resolution of the IR satellite dataset, ATYs with the annular phase lasting less than 3 h have been neglected; thus, the actual occurrence of ATYs may be higher. Furthermore, there are also some typhoons with typical annular features visible in the IR images, such as Abe (1993) and Melor (2009), that are not identified as ATYs because microwave images show that there are moderately organized spiral rainbands under the cirrus canopy. The averaged duration of the annular phases is about 24 h, and the longest annular state can last for 87 h [Typhoon Jelawat (2000)]. The averaged intensity during these annular phases is close to 110 kt, which is very similar to the intensity of category 4 typhoons (based on the Saffir–Simpson hurricane scale). Most of the ATYs occurred from August to October, corresponding to the main typhoon seasons in the WNP.

Figure 1 shows IR images of all ATYs listed in Table 1. During each annular phase, a clear, circular, and normal-to-large-sized eye is surrounded by a nearly symmetric annulus of deep convection in the color-enhanced IR

TABLE 1. A list of annular typhoons in the WNP from 1990 to 2009, including the dates during which they exhibited annular typhoon characteristics, the number of hours they exhibited annular typhoon characteristics, the intensity range these typhoons experienced during each annular phase, the times and locations of the first landfalling after annular phases, and the formation region of annular phases. Note: regions R1 and R2 are defined in Fig. 5.

	Storm (year)	Annular period (calendar)	Duration (h)	Intensity range (kt)	Landfalling time	Landfalling locations [lat (N), lon (E)]	Landfalling nations/regions	Formation region
1	Walt (1991)	2100 UTC 13 May–2100 UTC 14 May	24	98–118				R1
2	Yvette (1992)	2100 UTC 14 Oct–0900 UTC 15 Oct	12	150–155				R1
3	Nestor (1997)	1200 UTC 11 Jun–1200 UTC 12 Jun	24	115				R2
4	Jelawat (2000)	1500 UTC 5 Aug–0600 UTC 9 Aug	87	80–100	1000 UTC 10 Aug	(29.3°, 121.9°)	China	R1
5	Man-Yi (2001)	0000 UTC 6 Aug–0600 UTC 7 Aug	30	95–115				R2
6	Sinlaku (2002)	0600–1200 UTC 4 Sep	6	90	1100 UTC 7 Sep	(27.3°, 120.4°)	China	R1
7	Parma (2003)	1800 UTC 23 Oct–0900 UTC 24 Oct	15	105–125				R2
8	Ma-On (2004)	0900 UTC 7 Oct–0000 UTC 8 Oct	15	90–140	0800 UTC 9 Oct	(35.2°, 139.4°)	Japan	R1
9	Longwang (2005)	1200 UTC 30 Sep–0600 UTC 1 Oct	18	120–125	2100 UTC 1 Oct	(23.7°, 121.6°)	Taiwan/China	R1
10	Kirogi (2005)	2100 UTC 15 Oct–0600 UTC 16 Oct	9	100–115				R1
11	Saomai (2006)	1200 UTC 9 Aug–0000 UTC 10 Aug	12	140	1000 UTC 10 Aug	(27.1°, 120.4°)	China	R1
12	Nari (2007)	1200 UTC 14 Sep–1500 UTC 15 Sep	27	93–125	1100 UTC 16 Sep	(34.8°, 127.6°)	South Korea	R1

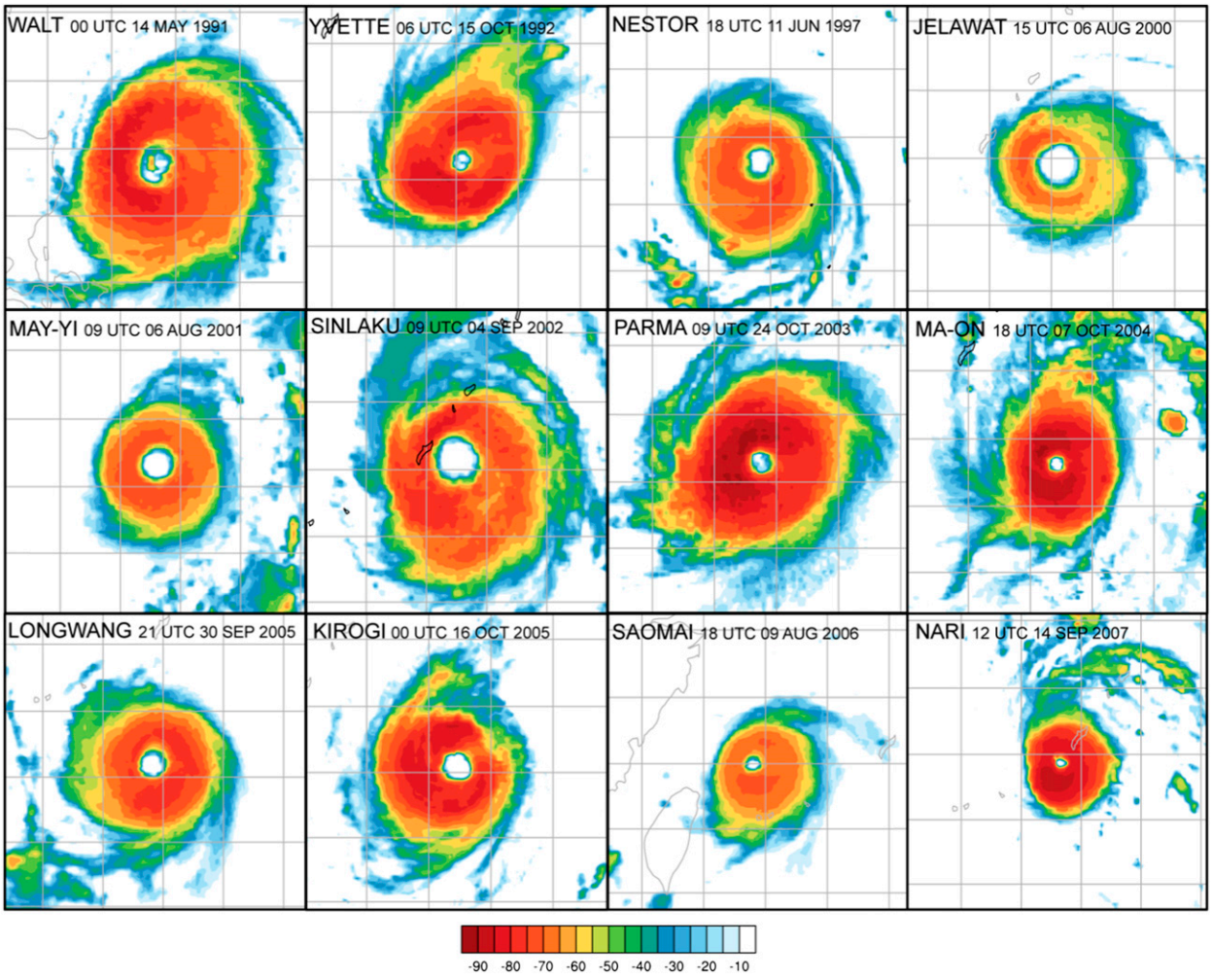

FIG. 1. IR satellite imagery for all 12 annular typhoons in the WNP at or near peak visual annular characteristics. The spacing for latitude–longitude lines is 28°.

satellite imagery (Fig. 1), which is a typical annular structure as defined in K03. In addition, deep convective features are generally lacking beyond the annulus of deep convection surrounding the eye. However, there is the possibility that spiral rainbands not visible in the IR imagery do exist under the cirrus canopy. Passive microwave can penetrate cloud and detect the rainbands under the cirrus canopy. For instance, Typhoon Abe (1993) and Typhoon Melor (2009) present typical annular features in IR images, while they present moderately organized spiral rainbands under the cirrus canopy in microwave images. Figure 2 shows the microwave images for each ATY if available during the annular phases. Microwave images also present a circular, large eye and symmetric eyewall convection for each ATY. Typhoon Kirogi (2005) has a small spiral rainband to the north of its eyewall; however, it is generally lacking when compared to the other intense tropical cyclones.

Time versus radius plots of the azimuthally averaged IR brightness temperatures for all 12 ATYs, as well as their intensity evolutions, are shown in Fig. 3. The boldface black lines indicate the beginning and end of each annular phase, and the gray lines mark the time when an ATY makes landfall. The most remarkable feature is the general lack of convection out of the broad eyewalls of the ATYs during their annular phases (Fig. 3). Moreover, clear and large eyes are also found during the annular phases. The eye sizes for ATYs show large differences, for instance, Jelawat, Man-Yi, and Sinlaku have relatively larger estimated eyes with radii of about 80–100 km during their annular phases, while Ma-On, Saomei, and Nari have relatively smaller estimated eyes with average radii of about 20–30 km. It can also be seen that there is a general lack of convection out of the broad eyewalls (Fig. 3).

Interestingly, most of the annular phases in the WNP occur after reaching maximum intensity, which is similar

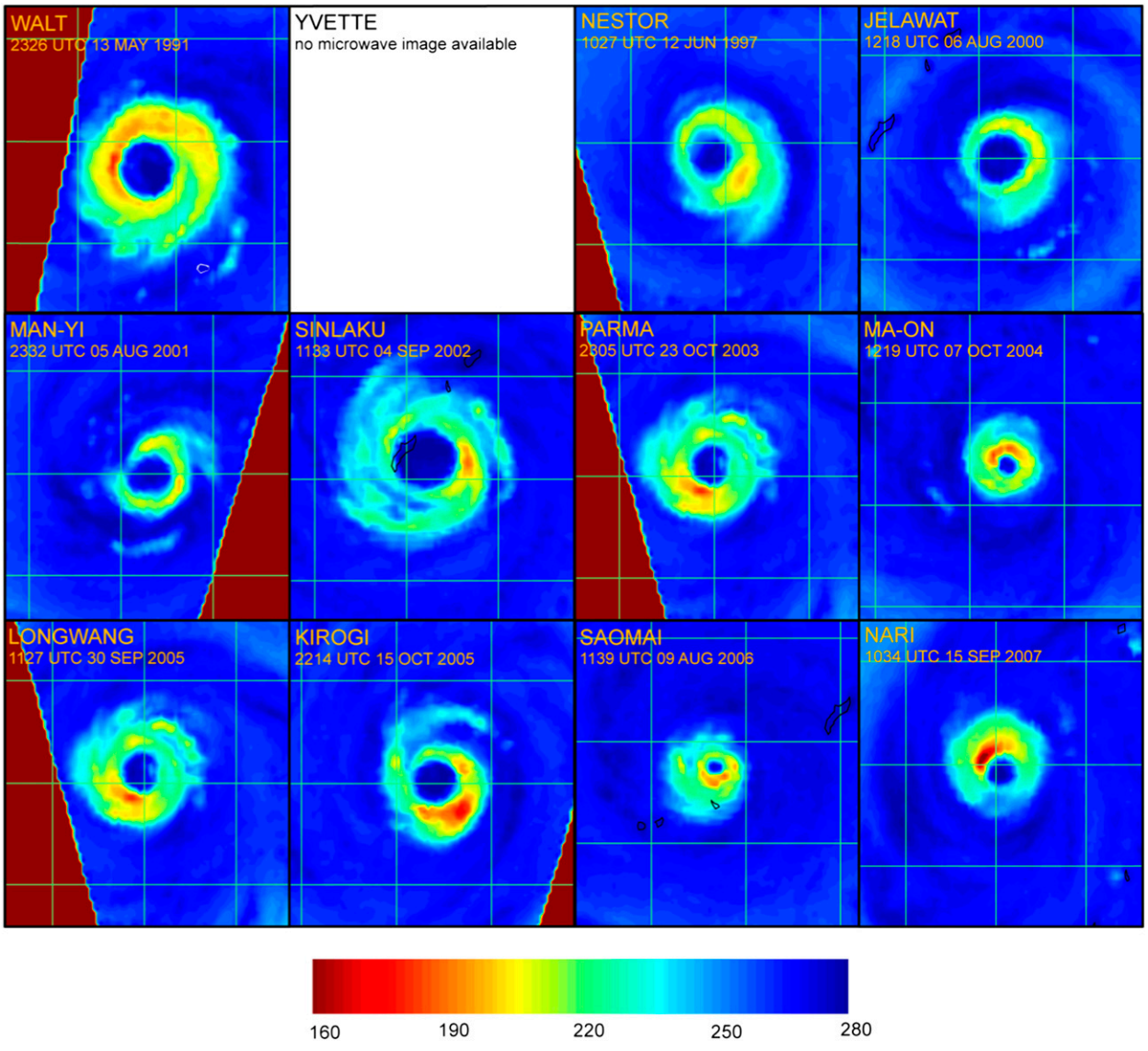

FIG. 2. Microwave satellite imagery for annular typhoons in the WNP during their annular states. The spacing for latitude–longitude lines is 2°.

to the eastern Pacific AHs (K03). As a result, ATYs have a slower filling/weakening rate after peak intensities, indicating a long and stable period of high intensity (Fig. 3). According to the definition of rapid intensification (maximum sustained surface wind speed increase of 30 kt over a 24-h period, hereafter RI) by Kaplan and DeMaria (2003), all 12 ATYs have experienced at least one RI event during their life cycles. The largest RI rate, which is about 70 kt within a 24-h period, appeared in the intensification phase of Typhoon Jelawat (2000).

Figure 4 shows composite time series of the normalized intensity for all 12 ATYs and the other nonannular WNP typhoons from 1990 to 2009 (excluding reports over land) in addition to the normalized intensity of the Atlantic storms that did not encounter cold water or make landfall as reported by Emanuel (2000), and the AHs reported by K03. Compared to the nonannular WNP typhoons composite, the ATY composite has a larger intensity tendency from −72 to −36 h, indicating ATYs intensify faster than the other WNP typhoons. During the following period prior to the peak intensity, the ATY composite is in general agreement with the other WNP typhoon composite. During the weakening stage, ATYs have a largely lower filling/weakening rate than the other WNP typhoons. In other words, ATYs tend to reach their peak intensities much faster and

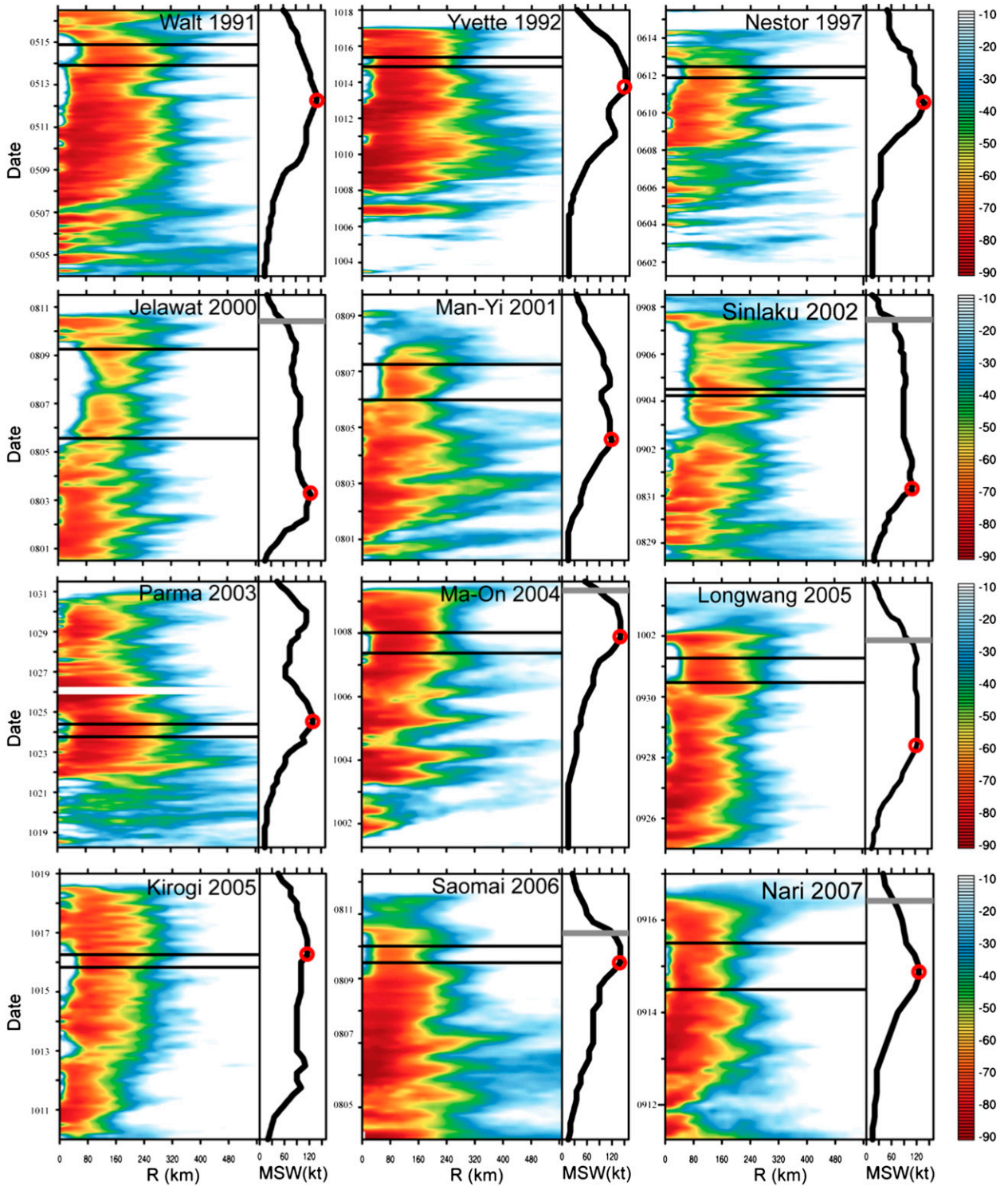

FIG. 3. Time vs radius plots of azimuthally averaged IR brightness temperature and the intensity for the entire life cycles of all 12 annular typhoons. Horizontal solid lines indicate the beginning and end of annular periods, the horizontal gray line indicates the time of first landfalling after annular phases, and the red circle indicates the peak intensity.

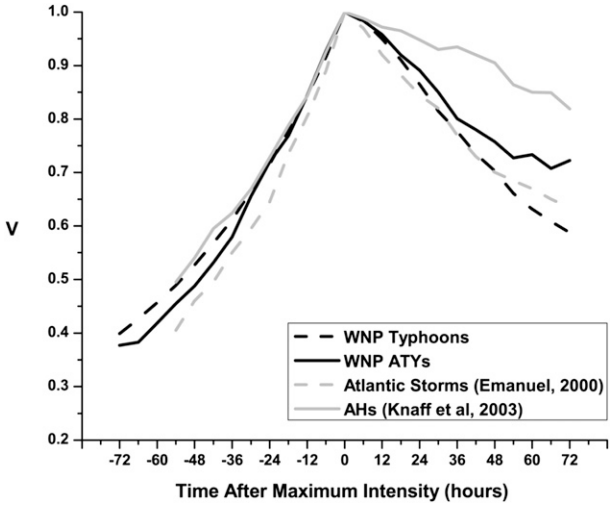

FIG. 4. Composite time series of the intensity (normalized by peak intensity) of TCs. The black solid and dashed lines represent, respectively, all 12 annular typhoons and the other 331 typhoons in the WNP (excluding the reports over land). The gray solid and dashed lines represent, respectively, the annular hurricanes reported by Knaff et al. (2003) and Atlantic storms that did not encounter cold water or make landfall (Emanuel 2000). Compositing is done relative to the time of the first peak intensity.

maintain their intensities much longer than nonannular WNP typhoons. Unlike the fact that ATYs intensify faster than nonannular WNP typhoons, the AH composite shows a consistently lower mean intensification rate than was found in Emanuel's (2000) composite prior to their maximum intensity (Fig. 4). Compared to the AHs, the ATYs have a relatively larger intensification rate from −54 to −36 h. Moreover, for ATYs, the averaged time between the maximum intensity and the annular phases occurring after maximum intensity is about 46 h, while the formation of AHs was in the mean very close to the time of maximum intensity. Furthermore, half of ATYs eventually made landfall, and their intensity weakened quickly when approaching the coast. As a result, ATYs present a larger filling/weakening rate than AHs.

The tracks of the 12 ATYs and the geographical distribution of their annular phases are shown in Fig. 5. Their tracks can be classified into three types, corresponding to the WNP's typhoon tracks in climatology (Wu et al. 2005). Although the occurrence of ATYs is independent of track types, the geographical distribution of the annular phases is limited in a narrow zonal belt between 20° and 30°N, which is located farther north than the AHs (Fig. 3 in Knaff et al. 2008). Moreover, there are two remarkable seedbeds for annular phase ATY occurrence between 120°–135°E (R1) and 140°–160°E (R2). There are nine ATYs in R1 in total, and six of them eventually made landfall. On the contrary, AHs are more likely in the tropics and well away from the U.S. mainland; thus, quite a few AHs make landfall (Knaff et al. 2008).

As shown in Fig. 5, tracks of the landfalling ATYs are almost straight, especially from the beginning of their annular phases. Hence, they can gain strength after a long journey over ocean and maintain their peak intensities when approaching the coast. The averaged time interval between the ATY's landfalling time and the ending of its annular phase is about 30 h. In particular, Typhoon Longwang (2005) and Typhoon Saomei (2006) made landfalls about 12 h after the ending of their annular phases. The mean intensity (~95 kt) of the six ATYs prior to landfall is comparable with a category 3 typhoon. As a result, ATYs can hit land with tremendous force (Table 1). For example, Typhoon Saomei (2006) is documented as the strongest landfalling typhoon to impact the Chinese mainland since 1949, with a record intensity of about 130 kt. When Longwang (2005) hit Taiwan, it broke the intensity record at the Hualian surface station. Obviously, landfalling ATYs are great threats to eastern Asia, which is quite different from the typical impact of AHs in the Atlantic and eastern-central North Pacific.

4. Typical environmental conditions for annular typhoons

The NCEP–NCAR reanalysis dataset is used to calculate the environmental conditions associated with the annular phase of ATYs in addition to the environmental conditions of all category 2 or greater WNP typhoons from 1990 to 2009 (hereafter named group one). For comparison purposes, we also calculate the environmental conditions of category 2 or greater WNP typhoons between 20° and 30°N and during the months of August–October (hereafter named group two). Table 2 lists the statistics of intensity, translation speed, SST over the TC center, and the other environmental conditions. The differences of the environmental means are statistically evaluated using a Student's t test and a 95% confidence level. Statistical significance of the means in Table 2 is highlighted in boldface.

First, the environmental means for ATYs are compared with the environmental means for group one typhoons. Compared with the other intense WNP typhoons, the environmental conditions for ATYs show significantly lower SSTs, larger westerly upper flow, larger westerly deep zonal wind shear, and smaller magnitudes of deep and shallow total vertical wind shears. Second, since ATYs tend to form in a narrow zonal belt between 20° and 30°N, and in the months of August–October, the

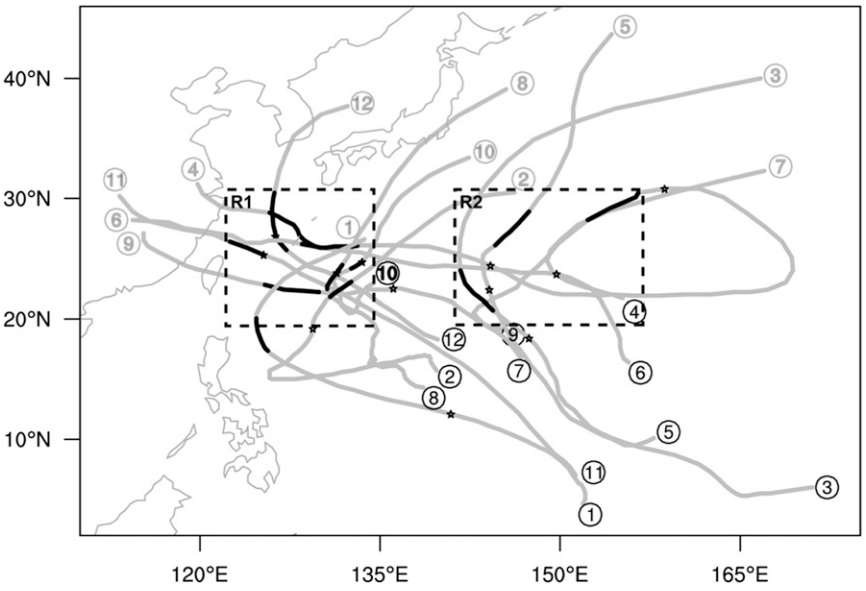

FIG. 5. The tracks of the 12 annular typhoons during 1990–2009 in the WNP. The annular phases are indicated by black portions of the tracks, and the star indicates the location of the peak intensity.

comparison between the environmental conditions for ATYs and the environmental conditions for typhoons in this region and during the months of August–October is more instructive. Compared with group two typhoons, the environmental conditions for ATYs also show significantly lower SSTs and larger magnitudes of deep total vertical shear. And the mean of the 200-hPa temperature for ATYs (−49.5°C) is significantly lower than that of group two typhoons (−48.7°C). Finally, there are no significant differences in the storm translation speed, shallow wind shears, and 200-hPa REFC (Table 2) between ATYs and group one/two WNP typhoons, indicating that the values of these factors are quite common for intense typhoons in the WNP. However, the values of 200-hPa REFC for all typhoons are quite small, suggesting the general lack of interaction between intense typhoons and the midlatitude upper-tropospheric trough.

TABLE 2. Statistics of the environmental conditions related to annular typhoons and other WNP typhoons. Listed are intensity; storm translation speed; SST; 200-hPa temperature and zonal wind; deep (200–850 hPa) total, zonal, and meridional wind shears; shallow (500–850 hPa) total and meridional wind shears; and 200-hPa storm REFC. Boldface font indicates statistical significance.

	Intensity (kt)	Speed ($m\,s^{-1}$)	SST (°C)	200-hPa T (°C)	200-hPa U ($m\,s^{-1}$)	Deep shear ($m\,s^{-1}$)	Deep U ($m\,s^{-1}$)	Deep V ($m\,s^{-1}$)	Shallow shear ($m\,s^{-1}$)	Shallow U ($m\,s^{-1}$)	Shallow V ($m\,s^{-1}$)	200-hPa REFC ($m\,s^{-1}\,day^{-1}$)
Annular typhoons (54 samples)												
Mean	108.9	4.5	27.7	−49.5	2.8	6.2	4.2	0.4	3.0	1.8	−0.2	−0.3
Std dev	17.3	2.4	0.7	1.1	4.9	3.3	3.0	4.7	2.0	2.3	2.2	2.3
Max	155	12.2	29.1	−47.5	14.5	17.0	10.9	13.6	8.5	6.6	5.7	4.2
Min	80	1.7	26.0	−51.7	−7.3	0.9	−1.8	−8.3	0.4	−2.3	−5.3	−9.0
Category 2 or greater typhoons (2952 samples)												
Mean	107.9	4.9	**28.3**	−49.2	**0.4**	**8.1**	**2.0**	0.4	**4.2**	1.2	0.2	−0.6
Std dev	17.8	2.6	**1.0**	1.4	**7.2**	**4.8**	**7.0**	6.1	**2.7**	4.0	2.6	3.6
Max	85	29.4	**30.9**	−44.0	**33.5**	**33.6**	**27.7**	28.1	**21.5**	16.9	13.3	23.2
Min	160	0.2	**21.6**	−52.8	**−19.9**	**0.1**	**−24.2**	−18.1	**0.0**	−11.5	−8.2	−43.6
Category 2 or greater typhoons (20°–30°N, Aug–Oct, 988 samples)												
Mean	105.7	4.5	**28.1**	**−48.7**	2.3	**7.7**	4.1	0.5	3.7	1.8	0.1	−0.2
Std dev	16.0	2.3	**0.8**	**1.4**	5.8	**4.8**	5.6	5.8	2.5	3.2	2.5	2.8
Max	85	17.1	**30.1**	**−44.0**	30.6	**26.3**	25.5	20.0	13.7	13.7	9.5	12.1
Min	150	0.2	**24.8**	**−52.4**	−19.9	**0.1**	−21.7	−13.9	0.2	−8.1	−8.2	−24.3

From the above comparisons, the thermodynamic factors (SST and upper-tropospheric temperature) and environmental dynamic forcing (vertical wind shear) are critical for the formation of ATYs. ATYs tend to form under the environmental conditions of specific SST range, a relatively cold upper troposphere, and weak westerly vertical shear. Statistics also show that the ranges of all the environmental factor values for ATYs are considerably smaller than those for both group one and group two WNP typhoons. Obviously, similar to AHs, ATYs only form under a specific combination of environmental conditions.

5. Annular typhoon formation and concentric eyewall replacement

The formation mechanisms of annular TCs are not clear so far. K03 reported that all the identified AHs underwent the mixing process with one or two possible mesovortices transforming a smaller eye into a larger one, and these transitions could be viewed as an eyewall replacement process. IR images show that Typhoon Parma (2003) and Typhoon Longwang (2005) experience a quite similar mixing process as Hurricane Howard (1998) discussed in K03, with two possible mesovortices transforming smaller eyes into larger eyes (figures not shown). As discussed in Wang (2008), the formation of annular hurricanes is closely related to the interaction between the inner spiral rainbands and the eyewall convection. Due to strong shear deformation and filamentation outside the eyewall, the cyclonic inward-moving inner rainbands experience axisymmetrization and evolve into a quasi-symmetric convective ring. This convective ring intensifies as it contracts while the eyewall breaks down and weakens and eventually replaces the original eyewall. Wang noted that this eyewall replacement process is very similar to the concentric eyewall replacement, except that there is no local maximum in the azimuthal mean tangential wind corresponding to the secondary convective ring. Zhou and Wang's (2009) numerical results also indicate that a concentric eyewall is an efficient route to forming an AH, and the storm can evolve into an AH within 24 h after the concentric eyewall replacement. Furthermore, based on observations, Kossin and Sitkowski (2009) hypothesized that the formation of a secondary eyewall, which reaches a quasi-steady state at a larger radius, is the precursor to annular hurricane formation. Thus, annular hurricane formation and eyewall replacement cycles might be viewed as similar phenomena that both begin with the formation of a secondary eyewall, but evolve somewhat differently after that.

Kuo et al. (2009) investigated the WNP typhoons with concentric eyewalls. They provide us with the full list of concentric eyewall cases in the WNP from 1997 to 2009 (H. C. Kou 2010, personal communication). There are 62 typhoons (69 cases) with concentric eyewalls between 1997 and 2009. Microwave images show that about one-fourth of all concentric eyewall replacement cycles can evolve into a clear large circular ring. But, due to moderate or heavy convection out of these rings, most of them cannot be identified as annular typhoons.

From 1997 to 2009, there are four cases with both annular phases and concentric eyewall cases: Jelawat, Man-Yi, Sinlaku, and Parma. Further analysis shows that only two annular phases (Jelawat and Man-Yi) are direct results of concentric eyewall replacements. For instance, Fig. 6 shows the evolution of a concentric eyewall into the annular phase of Typhoon Man-Yi (2001). At 1137 UTC 5 August 2001, the inner eyewall was surrounded by a circular secondary eyewall separated by the moat region (Fig. 6a); 12 h later, the inner eyewall dissipated and the secondary eyewall contracted moderately into a symmetric circular ring (Fig. 6b). The concentric eyewall of Typhoon Parma (2003) occurred after its annular phase, and the concentric eyewall case of Typhoon Sinlaku (2002) eventually evolved into a large circular ring, but with an organized outer rainband surrounding about two-thirds of the inner eyewall (figures not shown). In fact, the annular phase of Typhoon Sinlaku (2002) occurred about 2 days after the concentric eyewall case. In addition, the annular phase of Typhoon Walt (1990) also results from the concentric eyewall replacement (figures not shown).

The above analysis shows that only a small portion of typhoons with concentric eyewalls can evolve into annular TCs, despite the large occurrence rate of concentric eyewall cases (Kuo et al. 2009). Although annular TC formation and eyewall replacement cycles have some similarities, the environmental conditions for them have apparent differences. In the conceptual convective instability C versus shear S phase space model discussed in DeMaria (2009), AHs occur in conditions of low values of C and low values of S, whereas secondary eyewall formation occurs in conditions of high values of C and low values of S. Therefore, concentric eyewall replacement is one of the effective pathways to the formation of an annular TC, but may not be the primary pathway.

6. Summary and conclusions

This study investigates the main characteristics of the annular typhoons in the WNP from 1990 to 2009, with the new global TC-centered infrared brightness temperature and microwave datasets (HURSAT-B1 and HURSAT-MW). The occurrence rate of ATYs is close to 4%, which is as low as that of annular hurricanes in the

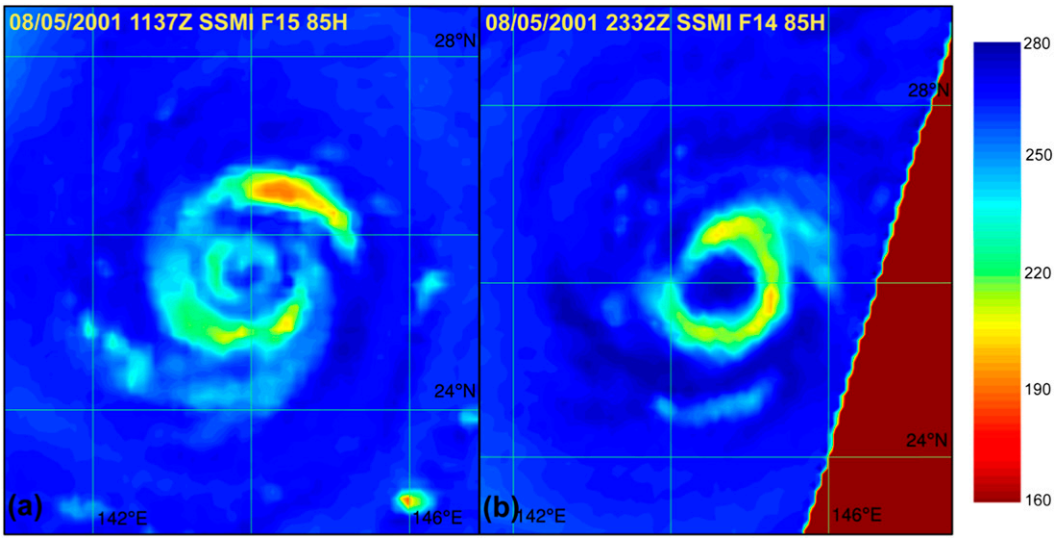

FIG. 6. Microwave imagery for Typhoon Man-Yi (2001). The spacing for latitude–longitude lines is 2°.

Atlantic and eastern-central North Pacific. Similar to AHs, ATYs are also intense TCs with average intensities of about 110 kt during their annular phases. Moreover, ATYs also intensify faster, maintain their peak intensities longer, and weaken more slowly than the other WNP typhoons.

The most remarkable difference between AHs and ATYs lies in their impacts on the coastal region. AHs are more likely in the tropics and well away from the U.S. mainland; thus, they seldom make landfall. Meanwhile, ATYs form within a narrow zonal belt between 20° and 30°N, and there are two seedbeds for the formation of ATYs, located east of Taiwan and central WNP, respectively. The former is located in the far west of the WNP basin, and is very close to the East Asia coastal region; as a result, six of the nine ATYs that formed in this region eventually made landfall. Moreover, the average duration between the time of landfall and the end of the annular phase of these ATYs is relative short, approximately 30 h, and then ATYs could maintain near peak intensities before landfalling. Two ATYs, Typhoon Longwang (2005) and Typhoon Saomei (2006), even made landfall immediately after their peak intensities. Therefore, the landfalling ATYs can hit the impacted regions with record intensities and pose a great threat to East Asia. Fortunately, ATYs also only form under a specific combination of appropriate environmental conditions. In particular, ATYs tend to form within a specific SST range (26.0°–29.1°C), in a relatively cold upper troposphere, and in the presence of weak westerly vertical wind shear.

The relationship between concentric eyewall replacement and annular phase formation is also discussed. Analyses on microwave images show that about one-fourth of concentric eyewall cases evolved into a larger circular ring; however, most of them cannot be identified as ATYs due to moderate or heavy convection out of the circular eyewalls. Only two annular phases are assumed as the direct results of concentric eyewall replacement. It is possible that the microwave data could have missed the formation of a secondary eye due to the spatial resolution of the instrument and the frequency of the observations. However, the analysis indicates that concentric eyewall replacement is one effective pathway in the formation of annular TCs, but may not be the primary pathway.

It can be seen that there were only three ATYs during the 1990s, whereas there were nine ATYs during the following decade. The environmental conditions for ATYs during these two decades are quite similar, except that the deep total vertical wind shear for category 2 typhoons between 20° and 30°N and in the months of August–October during the 1990s is significantly larger than that of the 2000s. Is the current climate more suitable for annular TCs in the WNP? This question is beyond the scope of this study, but deserves further investigation. To further improve the forecasts of ATYs, it is necessary to understand how the axisymmetric structure of an annular TC forms and is maintained under the complex environmental conditions in the WNP. Can we anticipate the formation of this relatively stable intense and long-lived structure? Future research will focus on the formation and maintenance mechanisms based on real-case numerical simulations and analyses.

Acknowledgments. We thank Dr. John Knaff for providing data for plotting the composited intensity traces for AHs and Atlantic storms, and Dr. Hung-Chi Kuo for

providing us the full list of concentric eyewall cases in the WNP from 1997 to 2009. We thank Drs. J. Song and S. Shu for the discussions and improvement of this manuscript and Ms. Lei Wu assistance with the calculation of the environmental conditions. The authors are also appreciated for the constructive and helpful comments from Dr. John Knaff and the other two anonymous reviewers. This research is sponsored by the National Natural Science Foundation of China under Grants 41130964, 41275055, 41275059, and 41105034. The SST data (NOAA_OI_SST_V2) are provided by the NOAA/OAR/ESRL/PSD, Boulder, Colorado.

REFERENCES

Bender, M. A., 1997: The effects of relative flow on asymmetric structures in hurricanes. *J. Atmos. Sci.,* **54,** 703–724.

DeMaria, M., 2009: A simplified dynamical system for tropical cyclone intensity prediction. *Mon. Wea. Rev.,* **137,** 68–82.

——, J. Kaplan, and J.-J. Baik, 1993: Upper-level eddy angular momentum fluxes and tropical cyclone intensity change. *J. Atmos. Sci.,* **50,** 1133–1147.

Emanuel, K., 2000: A statistical analysis of tropical cyclone intensity. *Mon. Wea. Rev.,* **128,** 1139–1152.

Frank, W. M., and E. A. Ritchie, 1999: Effects of environmental flow upon tropical cyclone structure. *Mon. Wea. Rev.,* **127,** 2044–2061.

——, and ——, 2001: Effects of vertical wind shear on the intensity and structure of numerically simulated hurricanes. *Mon. Wea. Rev.,* **129,** 2249–2269.

Jones, S. C., 1995: The evolution of vortices in a vertical shear. Part I: Initially barotropic vortices. *Quart. J. Roy. Meteor. Soc.,* **121,** 821–851.

Kalnay, E., and Coauthors, 1996: The NCEP/NCAR 40-Year Reanalysis Project. *Bull. Amer. Meteor. Soc.,* **77,** 437–471.

Kaplan, J., and M. DeMaria, 2003: Large-scale characteristics of rapidly intensifying tropical cyclones in the North Atlantic basin. *Wea. Forecasting,* **18,** 1093–1108.

Knaff, J. A., J. P. Kossin, and M. DeMaria, 2003: Annular hurricanes. *Wea. Forecasting,* **18,** 204–223.

——, S. A. Seseske, M. DeMaria, and J. L. Demuth, 2004: On the influences of vertical wind shear on symmetric tropical cyclone structure derived from AMSU. *Mon. Wea. Rev.,* **132,** 2503–2510.

——, T. A. Cram, A. B. Schumacher, J. P. Kossin, and M. DeMaria, 2008: Objective identification of annular hurricanes. *Wea. Forecasting,* **23,** 17–88.

Knapp, K. R., and J. P. Kossin, 2007: A new global tropical cyclone data set from ISCCP B1 geostationary satellite observations. *J. Appl. Remote Sens.,* **1,** 013505, doi:10.1117/1.2712816.

Kossin, J. P., and M. Sitkowski, 2009: An objective model for identifying secondary eyewall formation in hurricanes. *Mon. Wea. Rev.,* **137,** 876–892.

Kuo, H. C., C. P. Chang, Y. T. Yang, and H. J. Jiang, 2009: Western North Pacific typhoons with concentric eyewalls. *Mon. Wea. Rev.,* **137,** 3758–3770.

Malkus, J. S., and H. Riehl, 1960: On the dynamics and energy transformation in steady-state hurricanes. *Tellus,* **12,** 1–20.

Merrill, R. T., 1988: Environmental influences on hurricane intensification. *J. Atmos. Sci.,* **45,** 1678–1587.

Miller, B., 1958: On the maximum intensity of hurricanes. *J. Meteor.,* **15,** 184–195.

Reynolds, R. W., N. A. Rayner, T. M. Smith, D. C. Stokes, and W. Wang, 2002: An improved in situ and satellite SST analysis. *J. Climate,* **15,** 1609–1625.

Wang, Y., 2008: Structure and formation of an annular hurricane simulated in a fully compressible, nonhydrostatic model—TCM4. *J. Atmos. Sci.,* **65,** 1505–1527.

Wu, L., B. Wang, and S. Geng, 2005: Growing typhoon influence on East Asia. *Geophys. Res. Lett.,* **32,** L18703, doi:10.1029/2005GL022937.

Zhou, X., and B. Wang, 2009: From concentric eyewall to annular hurricane: A numerical study with the cloud-resolved WRF model. *Geophys. Res. Lett.,* **36,** L03802, doi:10.1029/2008GL036854.